ISSN 0747-9239, Seismic Instruments, 2017, Vol. 53, No. 1, pp. 1–18. © Allerton Press, Inc., 2017.
Original Russian Text © S.V. Poliakov, B.I. Reznikov, A.V. Shchennikov, E.A. Kopytenko, B.V. Samsonov, 2016, published in Seismicheskie Pribory, 2016, Vol. 52, No. 1, pp. 5–27.

The Range of Induction-Coil Magnetic Field Sensors for Geophysical Explorations

S. V. Poliakov[a, *], B. I. Reznikov[a, **], A. V. Shchennikov[a, *], E. A. Kopytenko[b, c, ****], and B. V. Samsonov[c, *****]**

[a] *Radiophysical Research Institute, Nizhny Novgorod, 603950 Russia*
[b] *Pushkov Institute of Terrestrial Magnetism, Ionosphere and Radio Wave Propagation, St. Petersburg Branch, Russian Academy of Sciences, St. Petersburg, 199034 Russia*
[c] *VEGA Geophysics Ltd., St. Petersburg, 192012 Russia*
**e-mail: SVP@nirfi.sci-nnov.ru*
***e-mail: bobrez@mail.ru*
****e-mail: scav110@inbox.ru*
*****e-mail: eugene.kopytenko@vega-geophysics.com*
******e-mail: boris.samsonov@vega-geophysics.com*

Abstract—This paper reports the long-term teamwork results obtained by an expert group from the Radiophysical Research Institute (NIRFI) and VEGA Geophysics Ltd. (VEGA, St. Petersburg) in the course of designing modern induction-coil magnetic field sensors. A comparative analysis of the world's most famous sensor models is carried out, and basic design and testing methods and features are considered. The range of low-noise induction-coil magnetometers (IMS-007, IMS-008, and IMS-009) designed by the authors for scientific and geophysical ground-based explorations is described. Research results are obtained from using the sensors for geothermal water exploration by broadband magnetotelluric sounding, investigation of the deep structure of the lithosphere by controlled source electromagnetic sounding, and monitoring of the Earth's natural electromagnetic field.

Keywords: induction-coil magnetometer, magnetotelluric sounding, Earth's variable magnetic field, ionospheric Alfven resonator

DOI: 10.3103/S0747923917010078

INTRODUCTION

Precision measurement of weak magnetic fields is a fast-paced branch of metrology widely used in both basic and applied research. The first experiments related to the high-accuracy low-frequency induction-coil magnetic field sensors were carried out at the Radiophysical Research Institute (NIRFI) in the first half of the 1980s and developed at a varying pace to date.

A new powerful shortwave station for ionosphere modification—the SURA facility—was commissioned in 1980. One of the most important problems at that time was the attempt to generate artificial geomagnetic pulsations under the impact of powerful modulated shortwave radio emissions on the ionosphere. An induction-coil magnetic sensor with a very low self-noise at frequencies close to or lower than the first Schumann resonance was designed and manufactured to record artificial signals. This sensor made it possible to reliably record short-period artificial geomagnetic pulsations.

In parallel, the conducted experiments resulted in identification of the so-called spectrum resonance structure (SRS) of the regular noise background related to the ionospheric Alfven resonator (IAR). In was established in further investigations that the SRS, along with the Schumann resonance, was a regular basic feature of the low-frequency noise background caused by thunderstorms. Since then, the regular electromagnetic noise background was recorded in digital form at the NIRFI investigation site *Novaya Zhizn'* (New Life) (settlement of Novaya Zhizn', Vorotynsky district, Nizhny Novgorod oblast). A special induction-coil sensor with a relatively narrow frequency band close to but somewhat lower than the first Schumann resonance, which was developed for monitoring purposes, has been operating to date. Pavel Petrovich Belyaev, a NIRFI scientist, has played a key role in the development of induction-coil sensors during the above-discussed studies.

When estimating the first work stage, it should in general be noted that the problem of receiving weak artificial signals required induction-coil sensors with

self-noise lower than the minimum regular background noise. This ensured the success of both active and passive experiments (the creation of artificial geomagnetic pulsations and SRS detection).

There is one more important problem that can be solved by "seeing" the minimum regular noise background in a very wide frequency range: so-called audio magnetotelluric sounding (AMT) of the Earth. In contrast to the above experiments, AMT imposes much more stringent performance and metrological requirements on induction-coil magnetic field sensors. That is why development of sensors for AMT purposes required testing and calibration in field conditions during real geophysical operations. This work was organized and performed by NIRFI in cooperation with VEGA Ltd. (St. Petersburg).

MODERN INDUCTION-COIL MAGNETOMETERS

Among the many types of magnetic field sensors, induction-coil sensors are distinguished by simplicity of design and manufacturing technology, availability of materials, and operational reliability. In recent years, considerable progress has been made in improving the metrological characteristics of induction-coil magnetometers and expanding their operational frequency range.

Induction-coil sensors are universal in occurrence on today's international market for magnetometry tools. Let us describe in brief the most common sensor models widely used in research and prospecting in Russia.

The German company Metronix (Metronix, 2015) offers a line of two wideband sensors such as the MFS-06 low-frequency sensor (Flyer-06e, 2015) and the MFS-07 high-frequency sensor (Flyer-07e, 2015). The specifications of the MFS-06 sensor are relatively unique in its class, and it can be used in a wide range of problems. Due to field reverse feedback, the sensor is characterized by a wide frequency range (from 1/4000 Hz to 10 kHz), high linearity of conversion, and transfer function stability, as well as by ultralow noise and the capability of internal calibration. The flat region of the amplitude–frequency characteristic (AFC) with excellent noise performance is in the range from 4 Hz to about 8 kHz. The sensor is 1250 mm in length with a diameter of 75 mm and a weight of 8.5 kg.

The MFS-07 higher-frequency induction-coil magnetometer is primarily designed to measure AMT and Earth sounding in the audio frequency band with a controllable source. Nevertheless, this device operates in a wide frequency range (from 0.001 Hz to 50 kHz) and can be used in standard magnetotelluric sounding (MT).

A MFS-07 sensor is characterized by extremely low noise, low temperature drift of input offset voltage and input offset current, and also by a very stable transfer function of temperature and time. The integrated calibration feature makes it easier to perform the sensor calibration by the user in the field conditions or testing of its transfer function. The AFC flat region starts from 32 Hz. The sensor is 800 mm in length at a diameter of 75 mm and weight of 5.5 kg.

The family of induction-coil magnetometers produced by a Canadian company Phoenix Geophysics (Phoenix_home, 2015; Phoenix_products, 2015) is represented by two types of wideband sensors such as low-frequency MTC-50 and high-frequency AMTC-30. The sensors are designed for operation in magnetotelluric production units produced by the same company. The specifications of these sensors given on the company's website are incomplete.

The MTS-50 low-frequency sensor is 1410 mm in length with a diameter of 60 mm. The sensor's frequency range is from 0.0002 to 400 Hz. As follows from the specifications of AFC and phase–frequency characteristics (PFC) given on the company's website, the sensor has no field feedback (FF), which results in considerable AFC and PFC irregularities, complicates data processing, and impairs the stability of its characteristics. The AMTC-30 high-frequency sensor is 820 mm in length with a diameter of 60 mm. The frequency range of this sensor is from 1 Hz to 10 kHz.

Products of the American company Zonge (Zonge, 2015) are represented by two types of sensors. The ANT/4 has the lowest frequency in the sensor range. It is 1380 mm in length with a diameter of 48 mm and a weight of 6.2 kg. In the AFC flat region of 0.1 Hz–1 kHz, the sensor has a sensitivity of 100 mV/nT. The ANT/6 is a medium-frequency and wideband sensor 910 mm in length with a diameter of 48 mm and weight of 3.2 kg; the AFC flat region is in the range from 10 Hz to 10 kHz. The ANT/5 is the smallest and lightest sensor in the line (610 mm in length with a diameter of 36 mm and weight of 1.5 kg) which is designed for measurements in the range of 0.25 Hz–10 kHz.

Magnetometers of the American company Schlumberger (Schlumberger, 2015) are represented by a line of four sensors, the BF-4, BF-6, BF-7, and BF-10, designed for work in different frequency ranges. The lowest-frequency BF-4 has an AFC flat region in the range from 1 to 700 Hz (operational range 0.0001–700 Hz) at a length of 1420 mm, diameter of 60 mm, and weight of 7.9 kg. The medium-frequency BF-10 is distinguished by a frequency range from 0.1 Hz to 10 kHz with the same dimensions and weight.

The LEMI sensors developed at the Lviv Center of the Space Research Institute, National Academy of Sciences and National Space Agency of Ukraine, are represented on the market by a relatively wide range of specialized transducers. The LEMI-120 (LEMI-120, 2015) magnetometer has extremely low noise and a wide dynamic frequency range, which makes it suit-

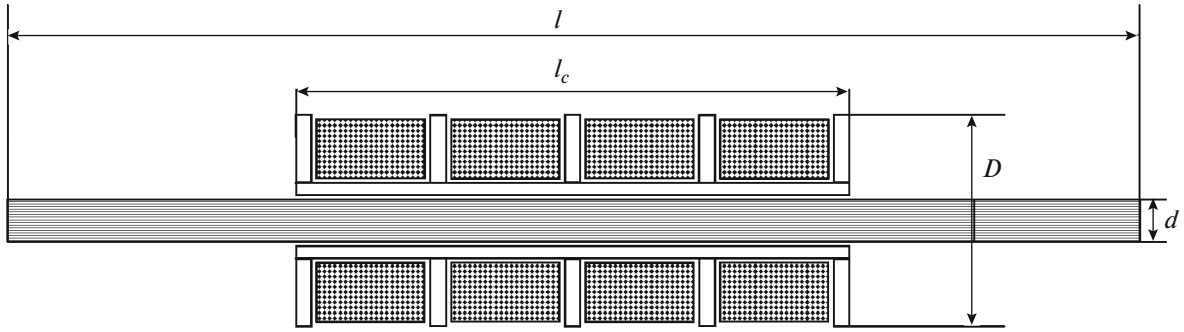

Fig. 1. Components of induction-coil magnetic field sensor.

able for various applications in geophysics. The LEMI-120 sensor is 1340 mm in length with a diameter of 85 mm and weight of 6 kg. It has a relatively high sensitivity and operates in the frequency range of 0.0001–1000 Hz. The LEMI-118 induction-coil magnetometer (LEMI-118, 2015) is a medium-frequency sensor for a frequency band of 1–70000 Hz. It is 800 mm in length and weighs 1.7 kg.

Russian high-class induction-coil magnetometers have occurred rarely on the Russian market to date. We can mention, e.g., a NV0195_7 sensor (NVLab, 2015) developed by the International Academy of Sciences of Ecology, Human and Environment Safety (St. Petersburg). It has a flat amplitude–frequency characteristic with a cutoff frequency of 0.5 Hz and a relatively low noise level, and thus can be used for exploration works by AMT. The sensor is placed in a watertight glass–fabric–plastic tubular housing 1110 mm in length, 70 mm in diameter, and 4.8 kg in weight. It is a basic model of the series united by common design solutions, which is designed to operate in the frequency range from 0.001 Hz to 20 kHz.

The highly sensitive KVVN-7 measurement station is described in (Kolobov et al., 2012). It uses Russian magnetic sensors and can provide equally effective frequency sounding with a controllable source and AMT in the field of natural variations in a wide frequency range (0.1–2000 Hz). Application of the KVVN-7 station allows high-resolution investigation of the electrical conductivity and fluid regime in the earth's upper crust to solve both geological problems and problems of electromagnetic monitoring of earthquake hazard areas in conjunction with seismic methods.

In recent years, NIRFI (Nizhny Novgorod) in cooperation with VEGA Ltd. (St. Petersburg) has developed advanced induction-coil sensors for geophysical studies in a wide frequency range, such as the IMS-007, IMS-008, and IMS-009. A detailed description of the designs and specifications of these sensors are given below.

BASIC METHODS AND SPECIFIC FEATURES OF THE DESIGN AND TESTING OF MODERN INDUCTION-COIL SENSORS

The induction measurement of the variable magnetic field is based on Faraday's law of electromagnetic induction. The ferromagnetic core distorts the measured magnetic field, concentrating magnetic force lines and, finally, increasing the magnetic flux linked with the measuring coil turns. Voltage U_S at the induction transducer output for external magnetic field H, which varies harmonically with a cyclic frequency ω, is specified by the following relationship:

$$U_S = i\omega\mu_{eff}\ \mu_0 N H_0 S. \quad (1)$$

In terms of design, the induction sensor is an inductance coil with a ferromagnetic core (Fig. 1) in one body with a preamplifier.

In Eq. (1) and Fig. 1, i is an imaginary unit; μ_{eff} is the effective magnetic permeability of the core, $\mu_0 = 4\pi \times 10^{-7}$ H/m is the vacuum magnetic permeability, N is the number of turns in the coil, l is the core length, l_c is the coil length, $S = \pi d^2/4$ is a cross-sectional area of the core, H_0 is the amplitude of the magnetic field strength, d is the core diameter, and D is the external coil diameter.

The effective magnetic permeability μ_{eff} of the core is defined not only by the magnetic permeability of the core material μ, but also by its geometrical dimensions, and to a greater extent. This can be explained with an electrostatic analogy or by the introduction of fictitious magnetic charges. The core is polarized in the external field H_0, and polarization charges arising at its ends decrease the field within the core. The exact solution of this problem is found only for an ellipsoid-shaped core (Bozorth, 1951):

$$\mu^*_{eff} = \frac{\mu}{1 + K(\mu - 1)}, \quad (2)$$

where K is a geometric factor determined by the following equation:

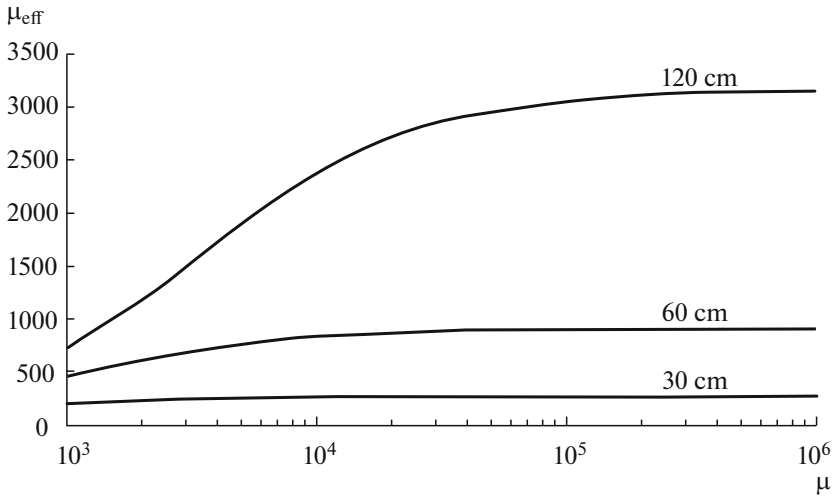

Fig. 2. Relation between effective magnetic permeability of core μ_{eff} and relative magnetic permeability of material μ at $l = 120$, 60, and 30 cm (core is 10 mm in diameter).

$$K = \left(\frac{d}{l}\right)^2 \left[\ln\left(2\,\frac{l}{d}\right) - 1\right]. \quad (3)$$

There is one more unaccounted-for parameter: the inhomogeneous magnetic field distribution along the sensor. The resulting solution corresponds to the core's central cross section, whereas the magnetic field induction decreases towards the ends. The multiturn measuring coil commonly takes up a significant length of the core, so formulas (2) and (3) are insufficient to calculate the sensor parameters. It is necessary to select the averaged value of μ_{eff} along the core occupied by the coil (only then is multiplication by the number of turns in formula (1) allowed).

Experimental verification has confirmed the correctness and high accuracy of the following engineering formula for the effective conductivity of the average current μ_{eff} obtained in (Zimin and Kochanov, 1985):

$$\mu_{eff} = \frac{\mu^*_{eff}\left[1 - 0.255\left(l_c/l\right)^2\right]}{1 + 0.975\left(\frac{S}{l^2}\right)\left[\ln\left(\sqrt{\pi\, l^2/S}\right) - 1\right]\left(\mu^*_{eff} - 1\right)}. \quad (4)$$

Based on the calculations performed by the above-mentioned formulas, the requirements for the material magnetic permeability are not too stringent, if the core is not very long. Fig. 2 shows the calculation data on the relation between μ_{eff} and material magnetic permeability μ for three core length values: 120 cm (low-frequency sensor), 60 cm (medium frequencies), and 30 cm (high frequencies). In all cases, the core diameter is 10 mm, while the coil occupies the half-length of the core and is arranged centrally.

According to the calculation results, the requirements on the material with respect to the magnetic permeability become more stringent with increasing core length/diameter ratio, and material with a permeability of tens of thousands should be used to achieve the maximum effective magnetic permeability of a "long" core with $L = 120$ cm (lowest frequencies).

In addition to the required high relative magnetic permeability, the core should not be characterized by heat losses caused by Foucault currents throughout the frequency band. This minimizes the sensor's electromagnetic noise related to the active component of its impedance. Historically, cores for inductive sensors were made from special grades of low-conducting ferrites (a ferrite core was used, e.g., in MFS sensors by Metronix). These cores are characterized by minimum heat loss, but the magnetic permeability values are not high enough (commonly, ~10000).

Materials with the above-mentioned properties are currently available. Laminated cores pressed from a thin ribbon of high-permeability (the hysteresis loop of the material should be as narrow as possible) amorphous alloys are the most frequently used (Ferrite, 2015).

Formula (1) includes $S_{eff} = \mu_{eff}S$, which specifies the degree of core concentration over the magnetic field; let us designate it effective area of the core. This value largely depends on the geometric dimensions of the core and coil.

Figures 3–5 show the relations of this value with the core length and diameter, as well as the filling factor of coil turns throughout the core $\chi = l_c/l$, respectively. According to the calculation results, an increase in core length is the most effective method to increase the sensor's output signal and, simultaneously, its sensitivity.

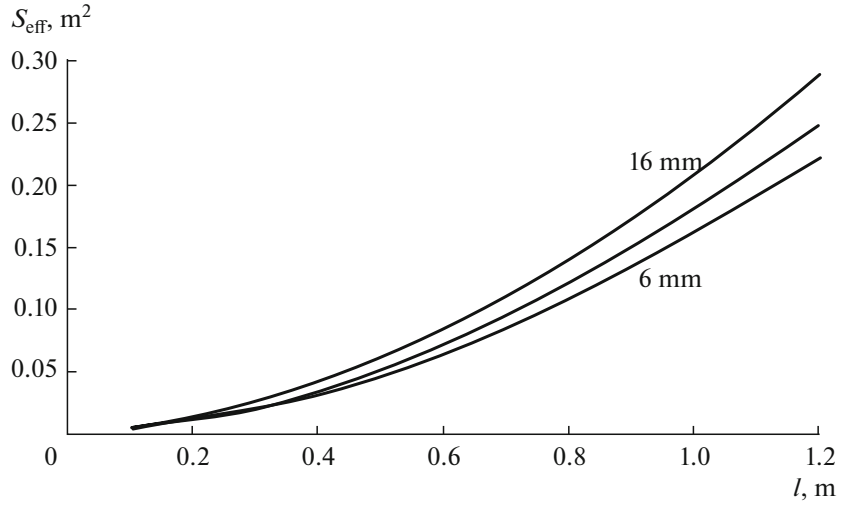

Fig. 3. Relation between effective area S_{eff} of core and its length (m) for core diameter of 6, 10, and 16 mm.

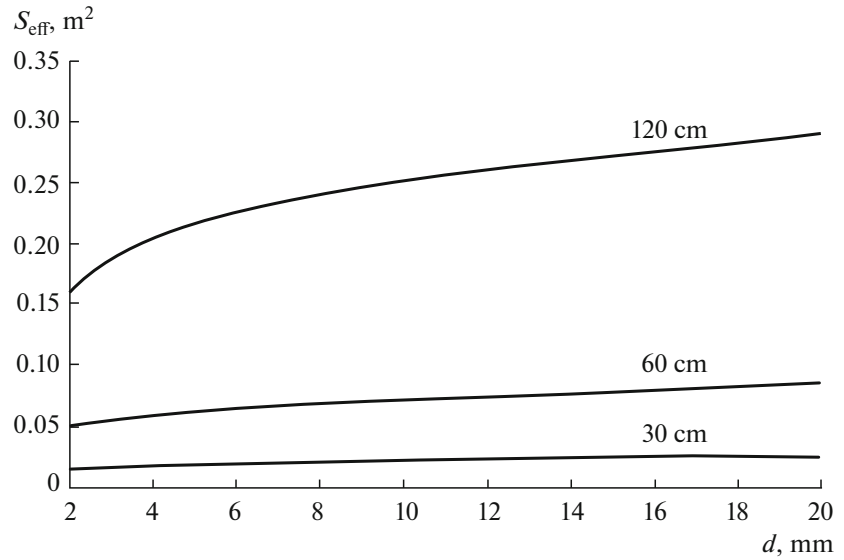

Fig. 4. Relation between effective area S_{eff} of core and its diameter (mm) for core length of 120, 60, and 30 cm.

In this case, a sensor's size and weight are natural limiters. It is extremely inconvenient to use big and heavy sensors for a long time in field conditions. The common low-frequency sensors are about 1 m in characteristic length and weigh 10 kg. Meanwhile, sensors permanently installed at research sites and scientific observatories should be longer.

According to Fig. 4, the effective area of the core and, simultaneously, the sensor's output signal level increases with the core diameter. However, this is not the best way to increase sensitivity, because this dependence is relatively weak, while a larger core diameter increases the diameter of receiver coil turns, coil resistance and, ultimately, noise.

Figure 5 is obviously indicative that it is necessary to strive for the minimum filling factor when developing a sensor. In the considered sensors, this parameter varies within $\chi = 0.3–0.6$. The number of turns N included in formula (1) is also one of the most important sensor parameters that defines its frequency properties (bandwidth), self-noise, and ultimate sensitivity.

In the curves shown in Figs. 3–5, there are regions of strong and weak dependences, which make it possible to obtain the optimum weight, size, and metrological characteristics of the developed sensors by varying these parameters.

The amplitude–frequency characteristic of an ideal sensor, according to Eq. (1), would be a linearly

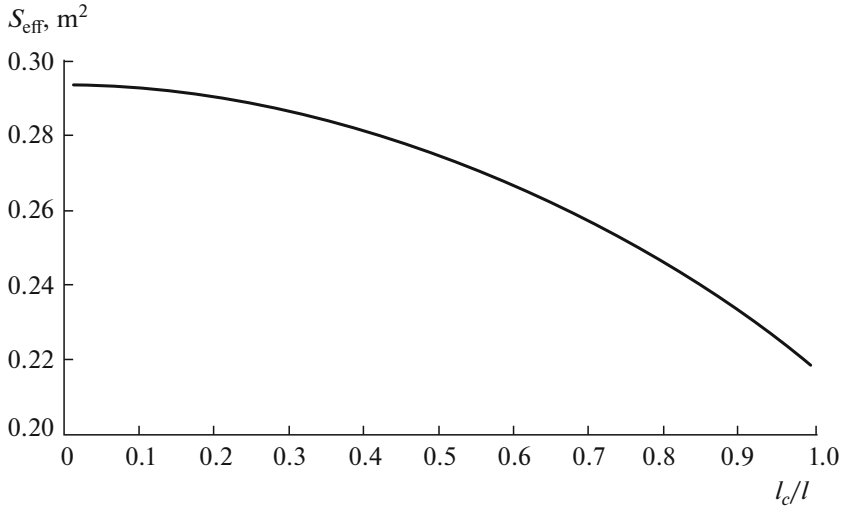

Fig. 5. Relation between core S_{eff} and filling factor $\chi = l_c/l$ for core 120 cm in length and 16 mm in diameter.

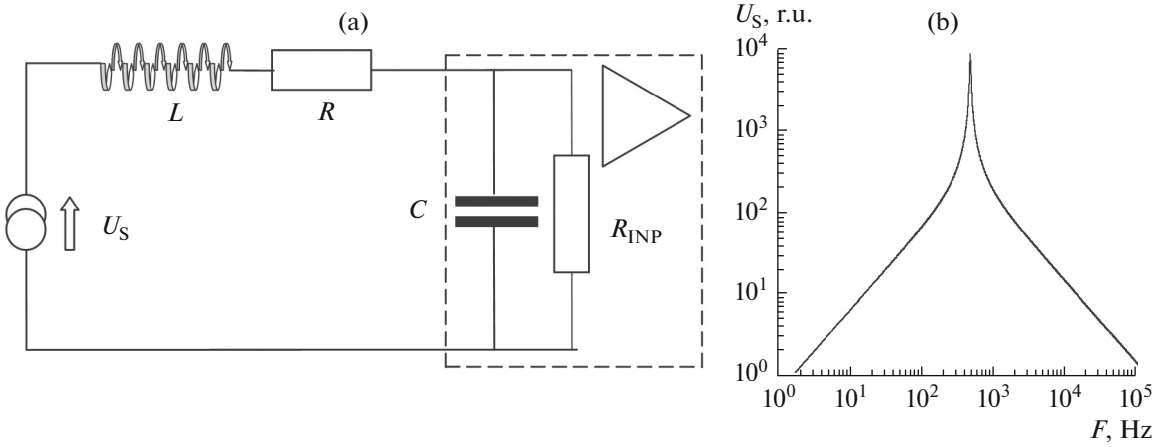

Fig. 6. Impedance scheme of sensor connected to amplifier (a) and AFC of sensor in arb. units (b).

increasing function with an absolutely flat phase characteristic and a constant phase shift $\pi/2$. However, this suggestion is valid only for the lowest frequencies. An increase in frequencies is accompanied by resonance phenomena in the electromagnetic circuit formed by the sensor's coil induction L and total capacity of the sensor's chain and amplifier's input $C = C_S + C_{INP}$.

The impedance connection scheme of the sensor and amplifier is shown in Fig. 6a. In this case, L is the coil inductance of the receiver, R is its active resistance, C_S is the distributed interturn capacity of the coil summed up with other parasitic capacities of the sensor (coil–core, coil–screen, etc.), and C_{INP} and R_{INP} are input capacity and resistance of the amplifier, respectively.

In this case, the components of the scheme have the following complex impedances forming a frequency-dependent voltage divider:

$$Z_L = i\omega L;\ Z_R = R;\ Z_C = 1/i\omega C,$$

$$Z_{INP} = Z_C R_{INP}/(Z_C + R_{INP}), \quad (5)$$

where Z_{INP} is the input impedance of the amplifier. The signal voltage right at the amplifier's input U_{INP} will be as follows:

$$U_{INP} = \frac{Z_{INP}}{(Z_L + Z_R + Z_{INP})} U_S = P(\omega)\, U_S, \quad (6)$$

where $P(\omega)$ is the complex frequency-dependent transfer ratio.

The AFC of the described sensors is a resonance curve (Fig. 6b) with a linear increase in amplitude with frequency at low frequencies and a drop at frequencies above the resonance caused by the parasitic capacity of winding and the input capacity of the amplifier. The final equation for the amplitude of the sensor's useful

signal reduced to the amplifier's input thus takes the following form:

$$U_{\text{INP}} = P(\omega)\omega\mu_0\mu_{\text{eff}}SNH_0. \quad (7)$$

When measuring the natural electromagnetic field in a wide frequency range, this characteristic yields some gain in the signal/noise ratio, because the natural electromagnetic noise has a well-defined frequency dependence in the form of $H_0 \sim 1/f^{\alpha}$. In the considered frequency range, α varies from 0.5 to 1.5. Based on these data, the requirements on the dynamic range of the receiving equipment at low frequencies are drastically reduced (Aleksandrov et al., 1972; Remizov, 1985).

Field feedback is applied to obtain a flat AFC in a wide frequency range, minimize the effect of the specific features of each certain sensor, and improve its performance. This technique is used in almost all modern inductive sensor designs.

Figure 7a shows the flow chart of such connection, while Figs. 7b and 7c show the AFC of the sensor for different gain factors and different resistance values in the feedback loop. Fig. 7d shows variations in the PFC of the sensor for variations in the feedback depth.

As follows from Figs. 7a–7d, the AFC of the sensor has a wide flat segment, which is convenient for processing the measurement results, but it causes nonlinearity in the PFC of the sensor (Fig. 7d).

The effects of the gain factor in the feedback loop and resistance element value in the feedback chain on the AFC of the sensor are somewhat different. A wider passband corresponds to a higher gain factor for a constant transfer ratio in the flat segment. An increase in the resistor resistance R_{FB} narrows the flat area while increasing the transfer ratio.

The complex transfer function of the sensor with an amplifier and field feedback is discussed in a number of works. Séran and Fergeau (2005) obtained the following equation for the sensor sensitivity (relation between signal amplitude at the amplifier output U_0 to the amplitude of variations in the magnetic field induction B_0):

$$\frac{U_0}{B_0} = \frac{-i\omega\mu_{\text{eff}}NSk_{\text{fb}}}{1 + i\omega\left(RC + \frac{k_{\text{fb}}M}{R_{\text{FB}}}\right) - LC\omega^2}. \quad (8)$$

In formula (8), k_{fb} is the gain factor in the feedback loop; R is an active resistance of the sensor coil; C is the total capacity at the amplifier input; L is the inductance of the sensor basic coil; R_{FB} is the resistance in the feedback chain, and M is the mutual inductance of the sensor coil and feedback coil depending on their design parameters and relation between the number of turns.

The frequency in Figs. 7b–7d is normalized with respect to the resonance frequency,

$$f_0 = \frac{1}{2\pi\sqrt{LC}},\ \omega_0 = 2\pi f_0, \quad (9)$$

while the flat AFC is distinguished by low-frequency and high-frequency drops along 0.707 at f_1 in the low-frequency region and at f_2 in the high-frequency region, related to the chain parameters as follows (Séran et al., 2005):

$$f_1 = \frac{R_{\text{FB}}}{2\pi k_{\text{fb}}M},\ f_2 = \frac{k_{\text{fb}}M}{2\pi R_{\text{FB}}L\,C}. \quad (10)$$

A number of semiempirical formulas with different correction factors are used to calculate the electrotechnical parameters of the chain. In (Tumanski, 2007), e.g., the sensor coil inductance and mutual inductance are calculated by the following relations:

$$\begin{aligned} L &= \mu_0\mu_{\text{eff}}\frac{N^2S}{l}\lambda, \\ \lambda &= 1.85 - 1.1\chi, \\ M &= \mu_0\mu_{\text{eff}}\frac{NN_{\text{FB}}S}{l}\lambda, \end{aligned} \quad (11)$$

where λ is the correction factor; χ is the core filling factor, and N_{FB} is the number of turns in the feedback coil.In the above-mentioned works, the authors report a number of empirical formulas to calculate the sensor capacities. Meanwhile, it should be noted that the main contribution to the total capacity at the preamplifier input is provided by the input capacity of the amplifier and high-frequency interference protection circuits of the sensor, yielding a total of about 200 pF.

Hence, the sensor sensitivity in the AFC flat segment can be estimated by the following simple formula (Séran et al., 2005):

$$\frac{U_0}{B_0} = R_{\text{FB}}\frac{l}{\mu_0N_{\text{FB}}\lambda}. \quad (12)$$

The ultimate sensitivity of the sensor on the flat segment required for optimum agreement of the sensor electronic circuit with the recording unit (ADC) over the dynamic range can be obtained by additional gain in stages after the feedback loop. If necessary, an additional frequency correction can also be introduced. The last stages of the preamplifier are commonly cable amplifiers with a differential output.

It should be noted that the sensitivity of the sensor, as well as its AFC, are accessory parameters determining the convenience of using a certain signal source at a specific measurement site characterized by local industrial noise. The most significant characteristic of the sensors is their ultimate sensitivity, i.e., the minimum signal level that this sensor can record. This characteristic is mainly defined by the sensor's self-noise. In general, device noise depends on the source and is characterized by its frequency spectrum. Let us briefly consider the main types of noise and parameters quantitatively characterizing their values.

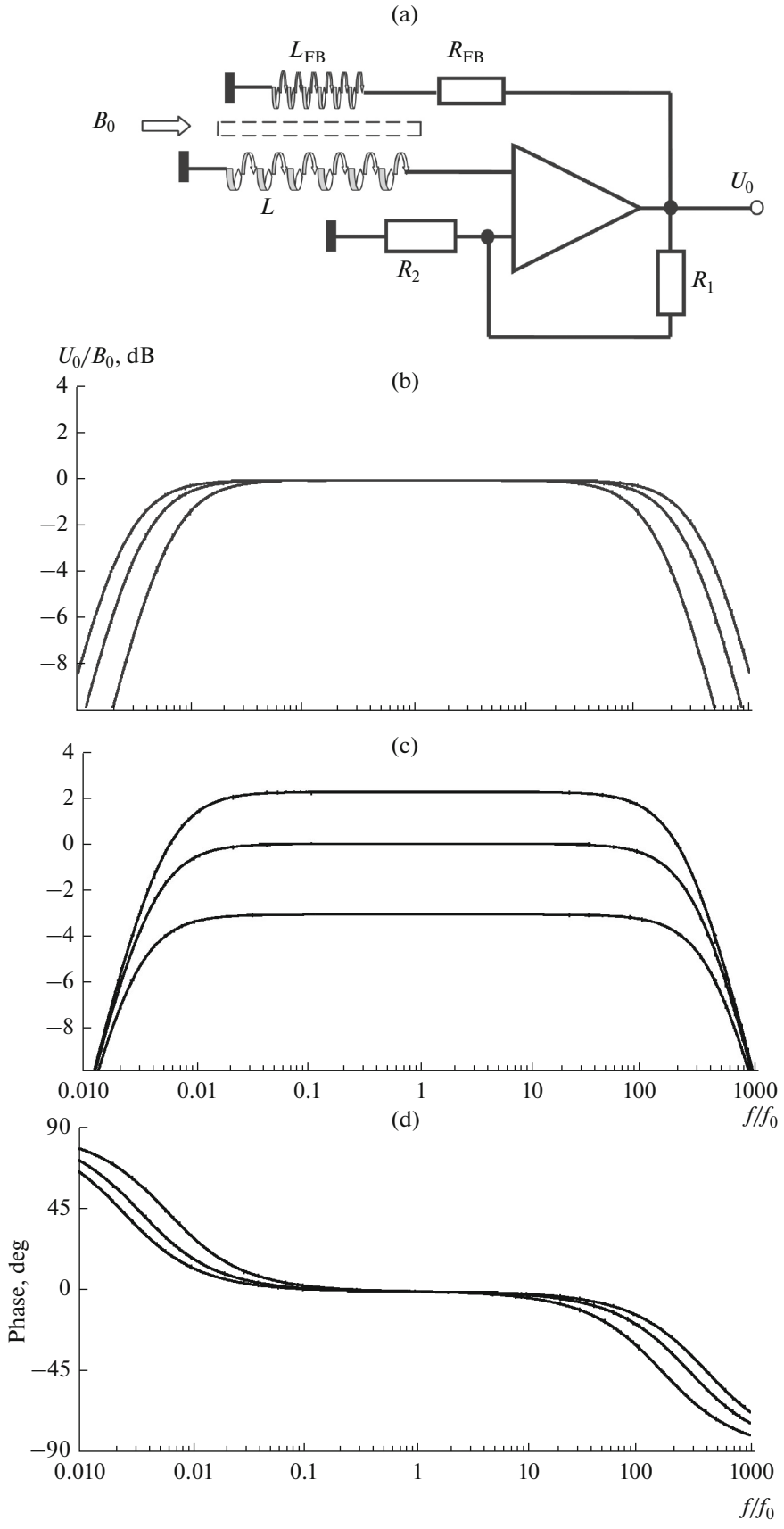

Fig. 7. Flow chart of feedback connection (a), AFC of sensor for different gain factors in feedback pool k_{fb} (b) and different values of resistor R_{FB} (c), and effect on PFC of sensor (d).

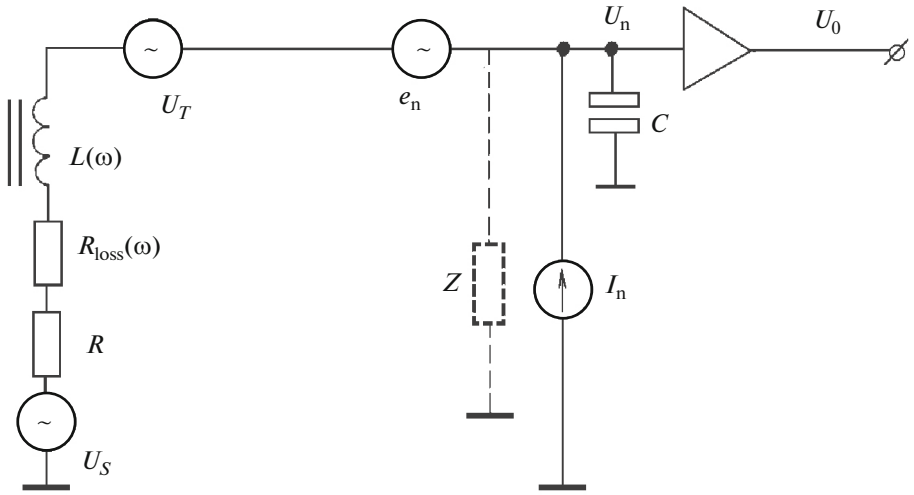

Fig. 8. Noise equivalent circuit of sensor with preamplifier.

The feedback affects both the useful signal and the amplifier input noise in the same way; therefore, in a first approximation, it has no effect on the signal/noise ratio and the limit parameters of the sensor can be obtained from the signal/noise ratio at the amplifier input using Eq. (7) for the amplitude of the useful signal.

Thermal Noise

Any resistor on the amplifier board, transistor p–n junction, sensor active resistance, etc., generate some noise voltage in a wide spectral range (white noise). The noise voltage in the open circuit is determined only by the active resistance R of source, and at temperature T the spectral density of thermal noise is determined by the following formula:

$$u_T = (4kTR)^{1/2}, \quad (13)$$

where $k = 1.38 \times 10^{-23}$ J/deg is the Boltzmann constant. At room temperature, $u_T = 1.27 \times 10^{-4}$ $R^{1/2}$ $\mu V/Hz^{1/2}$; e.g., for $R = 10$ kOhm, the rms voltage noise is about $u_T \sim 13$ nV/Hz$^{1/2}$.

Thermal noise related to thermal losses in the core until recently have been the main factor limiting the capabilities of sensors at high frequencies, because due to the skin effect, the effective permeability of the core becomes complex, while thermal losses are determined by the so-called loss tangent in the core:

$$\tan\delta_{loss} = \frac{\mathrm{Im}(\mu_{eff})}{\mathrm{Re}(\mu_{eff})}. \quad (14)$$

In this case, $R_{loss} = \omega L \tan\delta_{loss}$ is added to the coil resistance R in the sensor impedance formula, while the corresponding noise voltage caused by thermal losses in the core is also calculated by Nyquist's formula (13) with replacement of R by R_{loss}. It should be noted that such losses should be estimated using the experimentally measured value for a particular core with its specifications and geometrical characteristics, rather than the rated loss tangent value (because it applies only to the material the core is made of).

The use of advanced materials in core manufacturing (ferrites, laminated cores made of thin amorphous alloy ribbons) have made it possible to considerably reduce the influence of such noise factors. According to the noise measurement data obtained for the used cores, thermal noise can be neglected up to a frequency of about 100 kHz.

Preamplifier Noise

Figure 8 shows the noise equivalent circuit of the sensor with a preamplifier. In this case, e_n designates the voltage noise source, subsequent relative to the input signal, while i_n is the noise of the amplifier input current, assumed to be ideal. Hence, the total noise voltage of the amplifier reduced to its input will be as follows (Z is the total impedance modulus of the sensor):

$$u_n = \left[e_n^2 + (Zi_n)^2\right]^{1/2}. \quad (15)$$

The terms in brackets in (15) are the input voltage of the amplifier noise and noise voltage generated by the amplifier input noise current passing through the source impedance. The voltage noise e_n is predominant for a low resistance of the signal source, while the current noise Zi_n is predominant for a high resistance. The values e_n and i_n are the parameters of the transistors and operational amplifiers used to construct the preamplifiers. They can be optimally selected by the development of the circuit design and selection of the base components and operating currents.

Because the induction-coil sensor refers to a source with a high internal resistance, field-effect transistors with a very low noise current are used as the preampli-

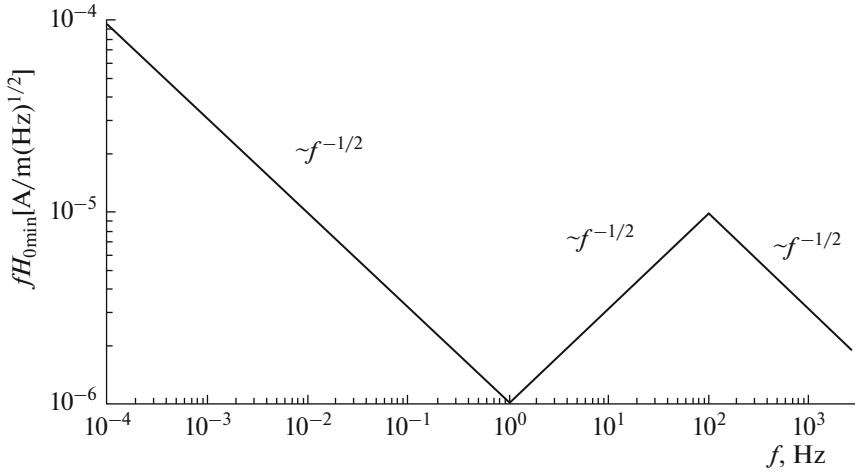

Fig. 9. Model of minimum geomagnetic background spectrum, reduced to preamplifier input. AFC of sensor with allowance for f factor.

fier input components (a few fA/(Hz)$^{1/2}$). In this case, the noise matching the sensor is reduced to selection of an input resistance value of the amplifier equal to its noise resistance $R_{INP} = e_n/i_n$.

Naturally this can only be done in a narrow frequency range, e.g., where there is a minimum in the spectrum of the natural geomagnetic field distorted by the frequency response of the induction sensor. Such a minimum in the frequency range 0.1–10 Hz was recorded in a generalization of long-term experimental data (Aleksandrov et al., 1972; Remizov, 1985). Figure 9 shows these results in graph form. The intrinsic noise effect is the most pronounced in the minimum region $f \sim 1$ Hz.

Various noise sources are irregularly distributed over the frequency range. For example, the low frequency range is dominated by amplifier voltage noise and thermal noise from the active resistance of the sensor, while high frequencies are dominated by the current noise of amplifier noise and thermal noise losses in the core.

Earlier, the flicker noise of linear amplifiers was a major factor limiting sensor capabilities at low frequencies. An attempt was made to solve this problem by developing parametric nonlinear amplifiers with signal modulation and demodulation ((MDM amplifiers), called choppers in the foreign literature and widely used by developers today. Continuous improvement in the circuit design of such amplifiers with application of new element bases have made it possible to reduce voltage noise to a few nV/(Hz)$^{1/2}$. Unfortunately, MDM amplifiers are characterized by high current noise (switching noise), resulting in high sensor noise at high frequencies. In modern sensors, MDM amplifiers can be disabled.

At high frequencies (over hundred Hertz), the modern linear amplifiers are characterized by typical voltage noise of 1.5–2 nV/Hz$^{1/2}$ at a current noise of a few fA/Hz$^{1/2}$. For reference, a current noise of the MDM amplifier is hundreds of fA/Hz$^{1/2}$. Due to the fact that all above-mentioned noise are not correlated, then the total noise voltage U_n is determined as follows:

$$U_n = \sqrt{e_n^2 + i_n^2 Z^2 + 4kT(R + R_{loss})}. \quad (16)$$

An ultimate sensitivity of the magnetometer with an amplifier is defined by the condition of equality of the useful signal at the amplifier input and total noise. Then, the minimum recorded signal can be calculated by the following formula:

$$B_{min}(f) = \frac{(e_n^2 + i_n^2 Z^2 + 4kT(R + R_{loss}))^{1/2}}{2\pi f \mu_{eff} NS}. \quad (17)$$

INDUCTION-COIL SENSORS FOR GROUND-BASED GEOPHYSICAL SURVEY: IMS-007, IMS-008, AND IMS-009. SPECIFICATIONS AND APPLICATIONS

Recent years have been marked by a range of advanced low-noise induction-coil magnetometers under the cooperation of NIRFI and VEGA Geophysics Ltd.: the low-frequency IMS-008 and medium-frequency wideband IMS-007 and IMS-009. These magnetometers are now successfully being used in both observatory observations and field works, including those in severe desert and Far North conditions.

Figure 10a shows an external view of the IMS-007 sensor set. The basic parameters of the IMS-007, IMS-008, and IMS-009 are given in the table.

The low self-noise of the magnetometer, with use of the gradient measurement method (Polyakov et al., 2006), make it possible to record signals whose ampli-

(a) (b)

Fig. 10. External view of IMS-007 sensor set (a) and preamplifier (b).

Specifications of IMS sensors

Sensor	IMS-007	IMS-008	IMS-009	Notes
Frequency range	0.001 Hz–10 kHz	0.0001 Hz–1 kHz	0.001 Hz–10 kHz	MDM disconnectable
AFC	(4–10 kHz) Flat	(2 Hz–1 kHz) Flat	(4 Hz–10 kHz)Flat	
	(0.001–4 Hz) Linearly increasing	(0.0001–2 Hz) Linearly increasing	(0.001–4 Hz) Linearly increasing	
Measured noise level	–	10^{-2} nT/Hz$^{1/2}$ per 0.01 Hz$^{1/2}$	2×10^{-2} nT/Hz$^{1/2}$ per 0.01 Hz	
		10^{-4} nT/Hz$^{1/2}$ per 1 Hz	2×10^{-4} nT/Hz$^{1/2}$ per 1 Hz	
		5×10^{-7} nT/Hz$^{1/2}$ per 1 kHz	10^{-6} nT/Hz$^{1/2}$ per 1 kHz	
Sensitivity	–	0.8 (V/nT) Hz (0.0001–2 Hz)	0.2 (V/nT) Hz (0.001–4 Hz)	
		1.6 V/nT (2 Hz–1 kHz)	0.8 V/nT (4 Hz–10 kHz)	
Output signal range	±10 V	±10 V	±10 V	±2.5 V (option)
Power consumption	60 mA (at 12 V)	65 mA (at 12 V)	40 mA (at 12 V)	
Dimensions:				
length	800 mm	1240 mm	800 mm	
diameter	75 mm	75 mm	65 mm	
Weight	6 kg	8 kg	6 kg	
Operation temperature	from –40 to +60°C	from –40 to +60°C	from –40 to +60°C	

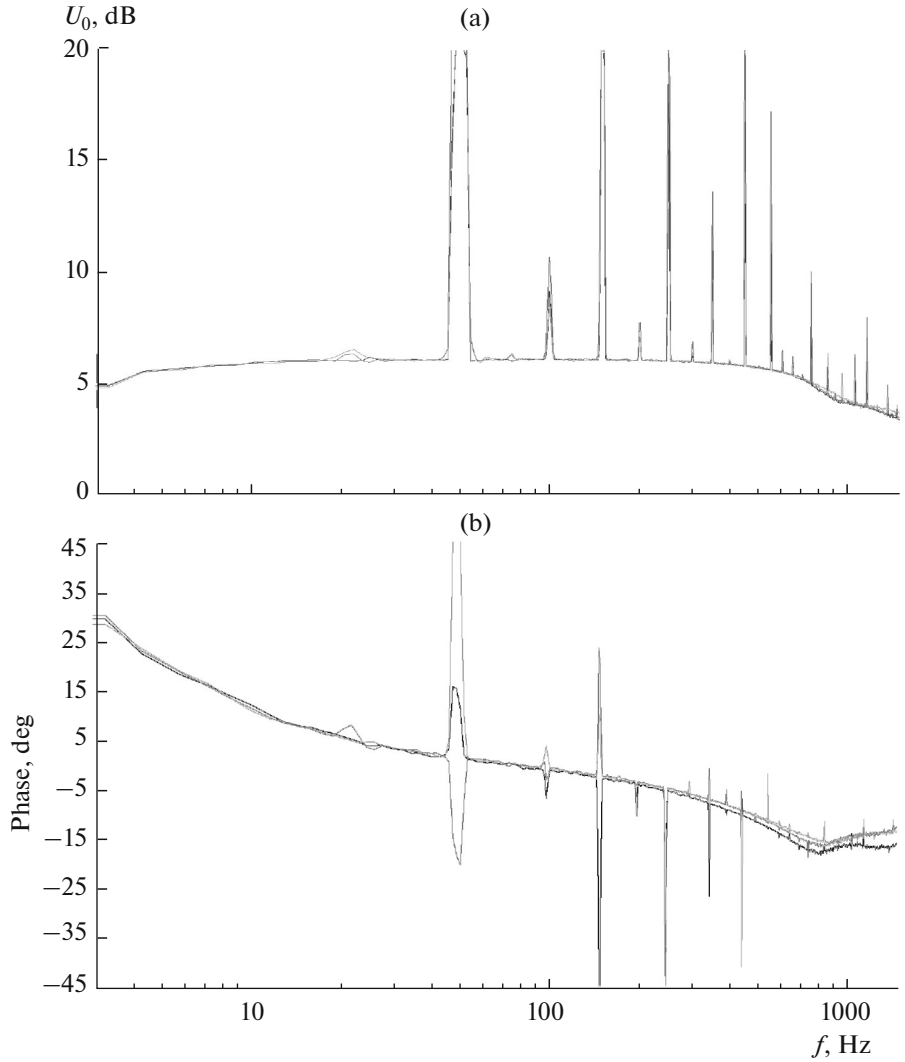

Fig. 11. AFC (a) and PFC (b) of three IMS-008 sensors measured using white noise.

tudes are much lower than the components of the natural noise background. When used together, the magnetometers make it possible to block the frequency range from 0.0001 Hz to 10 kHz. Such a broad high-frequencies band is achieved with laminated amorphous alloy cores, sectional coils, and other design features; as for the low frequency range, with low-noise MDM amplifiers. The integrated calibration feature simplifies verification of the magnetometer transfer function directly in experimental conditions.

The sensors are in durable waterproof glass–fabric–plastic tubes. For mechanical impact protection, the casing is covered with heat-shrinkable tubing. The housing is sealed on both sides by plugs, one of which has a connector for cable connection. A low-noise preamplifier and buffer amplifier with a differential output are installed in the common housing with a transducer (Fig. 10b) and are connected through a connector cable to the recording system and power source.

Sensor Testing and Verification Methods

Sensor testing and verification involve laboratory measurements of amplifier noise and preliminary rough adjustments of sensor sensitivity and the AFC. The final sensor parameters are set at testing sites with low industrial noise. Helmholtz coils or a magnetic dipole-type emitter installed at a distance of 20–50 m from the stand-mounted sensors are used as the known field source.

Accurate measurements of the sensor sensitivity, AFC, and PFC are carried out at several points of the operating frequency range. The sensors are irradiated with white noise in order to identify possible specific features of some sensors throughout the frequency range. Calibration using white noise is a convenient

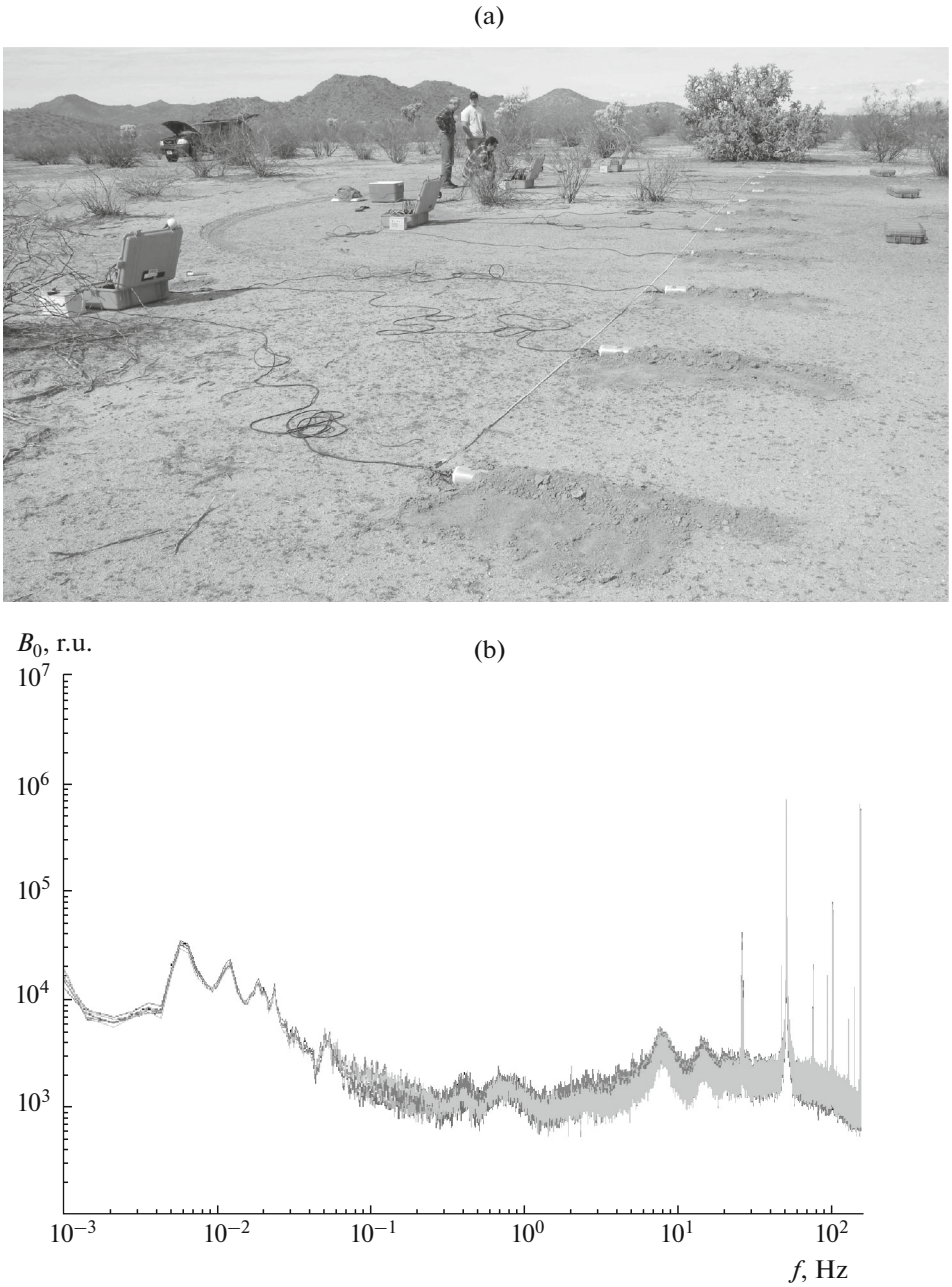

Fig. 12. Example of parallel testing of IMS-007 sensors on natural background (a) (Arizona, USA); (b) spectral density of natural electromagnetic field measured with six sensors installed in parallel.

and fast method for high-quality comparison of sensor performance throughout the frequency band. Figures 11a and 11b show the testing results obtained for three IMS-008 sensors using white noise.

Testing at an investigation site is completed by parallel testing, when a series of identical sensors are mounted on the stand or on the ground in parallel to each other with simultaneous recording of a natural or artificial background signal. These tests are also carried out in field conditions before any large-scale geophysical surveys.

Figure 12a shows an example of parallel testing for 12 IMS-007 sensors before exploratory electric surveys in the desert, while Fig. 12b shows the comparison data on the AFC of 6 IMS-007 sensors after parallel testing.

In addition to the standard laboratory and field tests related to a sensor's AFC and PFC measurements, a few IMS-008 magnetometers passed metrological testing in the Industrial Research and Methodological Metrological Center of the Federal National Unitary Research and Development Enterprise

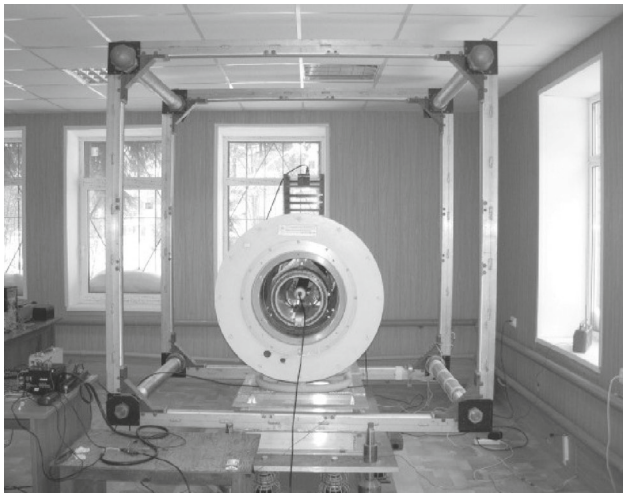

Fig. 13. Calibration bench in Federal National Unitary Research and Development Enterprise Geologorazvedka.

Geologorazvedka (Geological Survey). The experimental objective was to specify the sensor frequency characteristics and to determine the actual sensitivity threshold of the developed induction-coil magnetometers and linearity of their conversion factor. The tests were carried out in a few stages using the screened two-component measure of magnetic induction (STMMI).

The nonmagnetic pavilion of the Industrial Research and Methodological Metrological Center of the Federal National Unitary Research and Development Enterprise Geologorazvedka is located 25 km from St. Petersburg. It was built in compliance with all regulations imposed on buildings of this type (Nechaev, 2006). The calibration system is installed on a cement base isolated from the floor of the pavilion (Fig. 13). A massive aluminum plate on which the Helmholtz coils are mounted is isolated from the basement through a complex system of mechanical vibration damping.

Within the uniform magnetic field generated by the Helmholtz coils are a measuring compensation ferroprobe magnetometer and a multilayer permalloy screen with additional adjustment windings. This structure makes it possible to suppress external magnetic fields in a wide frequency range in the region intended for the test object by a factor of more than 10^3.

A known magnetic field with a specified frequency is generated for the tested magnetometer in a "purified" container simultaneously with suppression of external fields. Figure 14 shows the measurement data on the AFC and PFC of the IMS-008 and IMS-008 magnetic sensors. The frequency characteristics of the well-known in Russia MTC-50 sensors produced by Phoenix are compared to those of the fluxgate magnetometer.

The conversion factor of the magnetic sensor was measured at several operating frequencies as a function of the input signal level. The deviation of the conversion factor from its average value, being a linearity characteristic of the measuring system, did not exceed 0.25% in the range of input signals from 5 pT and over.

The greatest difficulties arise when measuring the such basic sensor characteristics as its ultimate sensitivity, i.e., the minimum useful signal that can be detected by the given magnetometer. This parameter is defined by the self-noise level of the sensor.

It should be noted that no such conventional testing techniques have been developed to date. These characteristics can be estimated, e.g., by subtracting output signals of two or more sensors after parallel testing. The time series obtained by subtracting the signals of two parallel sensors is the sensor self-noise and uncorrelated noise, e.g., parasitic wind, rain, and seismicity signals of different origin. Thus, it is possible to obtain an upper-bound estimate (somewhat understated) for the ultimate sensitivity of the magnetometer.

We managed to directly estimate the self-noise of the tested sensor on the stand with considerable suppression of existing industrial noise, as well as variations in the natural magnetic field. The average spectral noise density of the IMS-008 magnetic sensor in the frequency range from 10 to 1000 Hz was max 12 $fT/Hz^{1/2}$.

Figure 15 shows an example of measuring a test signal with a frequency of 7.8 Hz at 1 pT on the noise background of the IMS-008 magnetic sensor in the STMMI. A noise signal of about 2.4 Hz corresponds to the metrological device's own mechanical vibration frequency.

It should be noted that the IMS-008 sensors have been uninterruptedly working for 2.5 years during the observatory observations. The works were completed with measurements of the sensors' AFC and PFC. It was revealed that the characteristics were retained with a very high accuracy (less than 1%). Based on the testing results and long-term operation in different climatic conditions, the IMS-008 and IMS-009 sensors are characterized by a high stability of their parameters, extremely low noise characteristics, very low temperature drift, and a stable transfer function with time and at different temperatures.

Applications of the Sensors

Currently, the induction-coil magnetic sensors are widely used in various fields of science and technology mainly due to their high sensitivity and broadband capabilities with relative ease of use. In comparison with other high-precision high-sensitivity magnetometers, such as superconducting quantum interference devices and quantum systems, which require additional complex functioning conditions, induction-coil

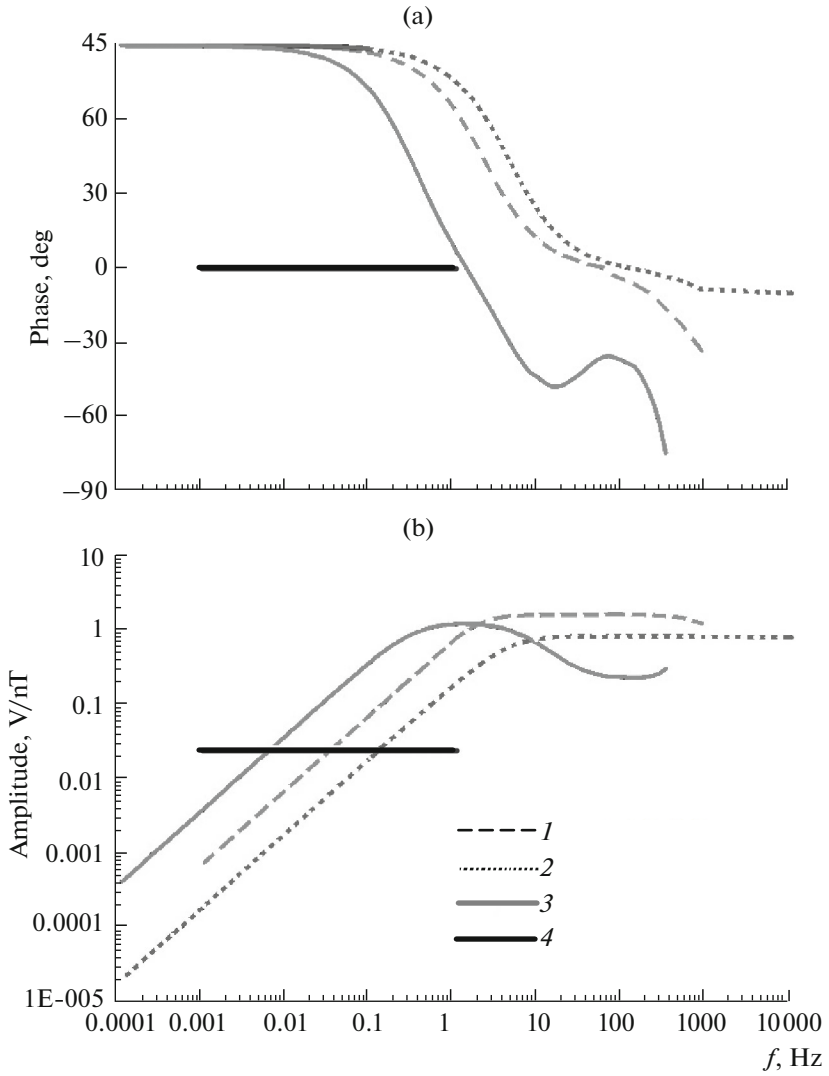

Fig. 14. PFC (a) and AFC (b) of IMS-008 (*1*), IMS-009 (*2*), Phoenix MTC-50 (*3*), and fluxgate (*4*) magnetometers.

magnetometers are very undemanding in terms of external circumstances. Because of these qualities, they are almost indispensable in present-day field geophysical and electric surveys.

These properties have made it possible to carry out electromagnetic sensing of the Earth's crust from a few hundreds of meters to tens of kilometers using only one type of sensor, thus considerably reducing the number of devices needed to conduct field works, on the one hand, and increasing the operational efficiency due to the lower number of required measurements, on the other. One of the major applications of induction-coil magnetometers in exploration geophysics is the search for geothermal waters using broadband MT. A number of such works with IMS-007 sensors can be found in (Dewhurst Group, 2015).

Figure 16 shows a pseudo-three-dimensional image of the apparent resistance distribution a the geothermal water discharge area, based on areal measurement results jointly obtained by Dewhurst Group (United States) and VEGA (Russia) using induction-coil magnetometers produced by VEGA in Nevada, United States.

Zhamaletdinov et al. (2013) have reported results obtained with IMS-008 magnetic induction-coil sensors during electromagnetic soundings with a controllable source. The objective was to study the deep structure of the lithosphere and to trace promising oil and gas horizons in the sedimentary cover of the West Siberian Platform in the Yamalo–Nenets Autonomous Okrug.

It should be noted that some academic research objectives related to the study of the Earth's low-frequency electromagnetic field cannot be achieved without induction-coil magnetometers.

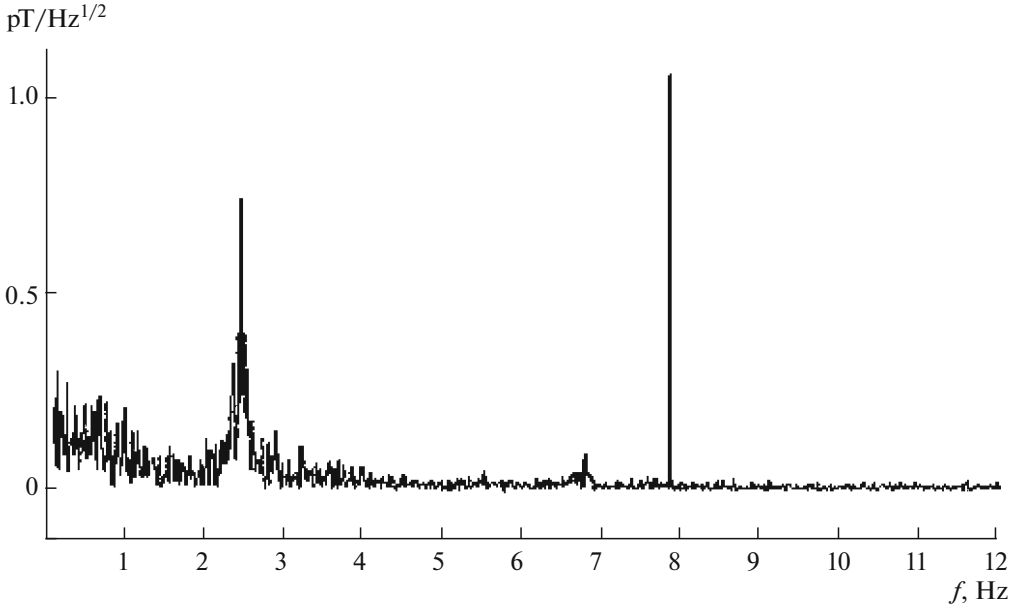

Fig. 15. Noise spectrum of IMS-008 magnetometer.

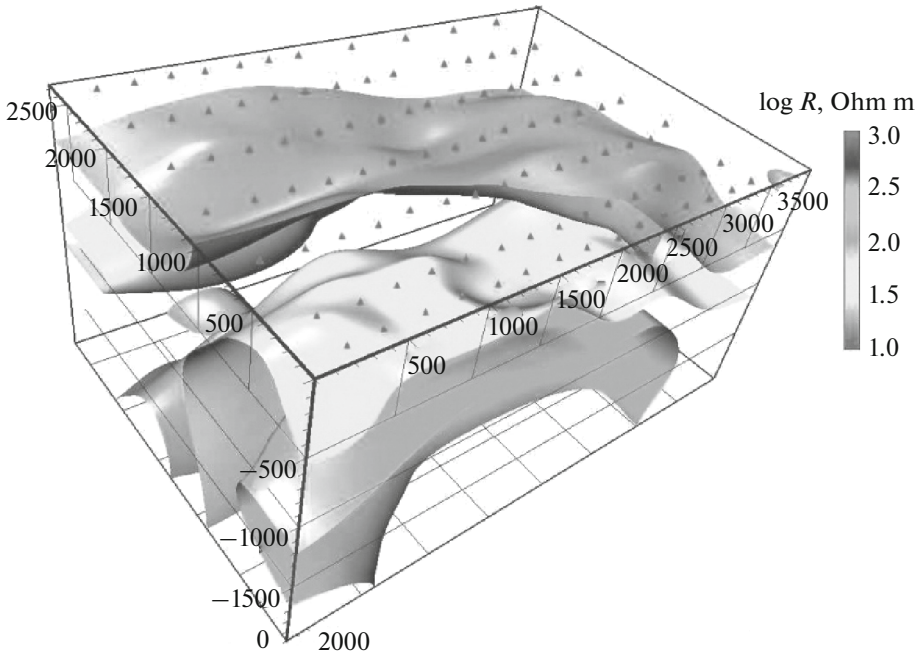

Fig. 16. Three-dimensional image of apparent resistance distribution near geothermal water discharge area obtained with IMS-007 sensors.

Figure 17 shows an example of a daily spectrogram of magnetic field variations in the frequency range up to 16 Hz, recorded by IMS-008 sensors in August 2010 at the Novaya Zhizn' investigation site. The figure clearly shows the frequency–time structure of the geomagnetic field with three Schumann resonances and well-traced specific features of the electromagnetic field such as the spectrum resonance structure (SRS) defined by the ionospheric Alfven resonator.

In its nature (frequency response of the induction-coil magnetometer and typical range of the natural background noise), an inductive sensor has the lowest signal/noise ratio at frequencies of about 1 Hz (Fig. 9), i.e., just at frequencies where SRS is observed. This

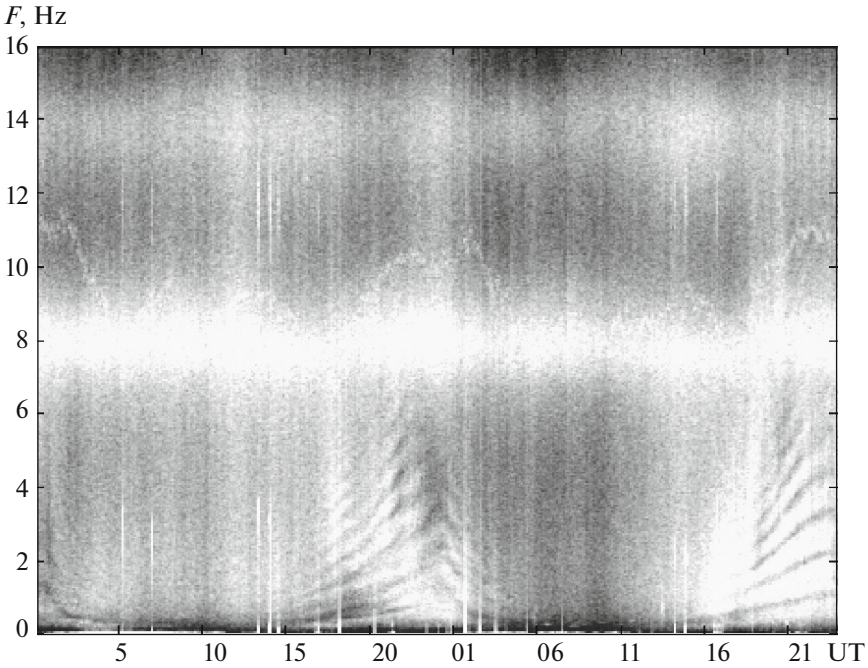

Fig. 17. Daily spectrogram obtained with IMS-008 sensors at Novaya Zhizn' site (Nizhny Novgorod oblast) on August 13–14, 2010.

means that regular SRS recording is a qualitative test of the induction-coil sensor for ultimate sensitivity. SRS provides data on the structure of the upper ionosphere and can be used in relevant diagnostics. For this reason, SRS is actively studied today in Russia and abroad.

Hence, problems of monitoring of the Earth's natural electromagnetic field for a variety of targets can be solved the most successfully using easy-to-handle sensitive broadband induction-coil sensors. Additional, more detailed examples of the observation results obtained with IMS-007, IMS-008, and IMS-009 sensors can also be found in (Kopytenko et al., 2010).

CONCLUSIONS

In addition to the presented range of induction-coil magnetometers, it is planned to develop a low-frequency sensor for frequencies $f \leq 30$ Hz with lower self-noise. This is aimed at gradient measurements (Polyakov et al., 2006) and measurements of the vertical magnetic field component. Judging by the modern development of equipment, we can assume that the best induction-coil magnetometers described above have achieved the fundamental technological limit of the physical parameters of magnetic induction transducers. This means that it is almost impossible to make a magnetometer with a much better quality using currently available materials and components. This applies to broadband induction-coil magnetometers for geophysical and other applications. Meanwhile, it is possible to design and manufacture magnetometers with substantially lower self-noise than those of the discussed magnetometers to solve other problems, e.g., those related to measurements in a relatively narrow frequency band.

REFERENCES

Aleksandrov, M.S., Bacleneva, Z.M., Gladshtein, N.D., Ozerov, V.P., Potapov, A.V., and Remizov, L.T., *Fluktuatsii elektromagnitnogo polya zemli v diapazone SNCh* (Fluctuation of the Terrestrial Electromagnetic Field in the ELF Range), Moscow: Nauka, 1972.

BF-4 magnetic field induction sensor, Schlumberger Company, 2015. http://www.slb.com/~/media/Files/rd/technology/product_sheets/emi_bf_4.pdf.

Bozorth, R.M., *Ferromagnetism*, Princeton, N.Y.: Van Nostrand, 1951.

Dewhurst Group, 2015. http://www.dewhurstgroup.us/ru/index.php/resources.

Field sensors, Phoenix Geophysics Company, 2015. http://www.phoenix-geophysics.com/products/sensors/?.

Flyer MFS-06e induction coil, brief description and specifications, Metronix Company, 2015. http://www.geo-metronix.de/mtxgeo/images/web/brochures/FlyerMFS-06e_en_v35.pdf.

Flyer MFS-07e induction coil, brief description and specifications, Metronix Company, 2015. http://www.geo-metronix.de/mtxgeo/images/web/brochures/FlyerMFS-07e_en_v35.pdf.

Kolobov, V.V., Kuklin, D.N., Shevtsov, A.N., and Zhamaletdinov, A.A., The KVVN-7 Multifunction digital measuring station for electromagnetic monitoring of seismoactive zones, *Seism. Instrum.*, 2012, vol. 48, no. 1, pp. 75–84.

Kopytenko, E.A., Palshin, N.A., Poljakov, S.V., Schennikov, A.V., Reznikov, B.I., Samsonov, B.V., New portable multifunctional broadband MT System, *IAGA WG 1.2 on Electromagnetic Induction in the Earth: Abstracts of 20th Workshop, Giza, Egypt, 2010.*

LEMI-118 induction magnetometer, brief description and specifications, Laboratory of Electromagnetic Innovations, 2015. http://www.lemisensors.com/?p=242.

LEMI-120 induction magnetometer, brief description and specifications, Lviv Centre of Institute for Space Research, 2015. http://www.isr.lviv.ua/lemi120.htm.

Magnetometers for geophysical surveys, Zonge International Company, 2015. http://zonge.com/instruments-home/instruments/sensors/.

Metronix Company, 2015. http://www.geo-metronix.de/mtxgeo/.

NV0195.7 alternating magnetic field transducer, 2015. http://www.nvlaboratory.spb.ru/0195.html.

Nechaev, S.A., *Rukovodstvo po statsionarnym geomagnitnym nablyudeniyam* (A Guide on Statonary Geomagnetic Observations), Irkutsk: Inst. Geogr. im. V.B. Sochavy Sib. Otd. Ross. Akad. Nauk, 2006.

Overview of properties of amorphous alloys, OOO NPP Astera, 2015. http://www.ferrite.com.ua/amorphous/.

Phoenix Geophysics Company, 2015. http://www.phoenix-geophysics.com/home/.

Polyakov, S.V., Reznikov, B.I., Shlyugaev, Yu.V., Kopytenko, E.A., First spatial discrimination of large-scale natural ELF interference: Case study of two-point measurements of the magnetic field produced by an artificial ionospheric source, *Izv. Vyssh. Uchebn. Zaved., Radiofiz.*, 2006, vol. 49, no. 12, pp. 1030–1042.

Remizov, L.T., *Estestvennye radiopomekhi* (Natural Radio Interferences), Moscow: Nauka, 1985.

Séran, H.C. and Fergeau, P., An optimized low-frequency three-axis search coil magnetometer for space research, *Rev. Sci. Instrum.*, 2005, vol. 76, 044502. doi 10.1063/1.1884026

Tumanski, S., Induction coil sensors: A review, *Meas. Sci. Technol.*, 2007, vol. 18, no. 3, pp. R31–R47.

Zhamaletdinov, A.A., Petrishchev, M.S., Shevtsov, A.N., Kolobov, V.V., Selivanov, V.N., Barannik, M.B., Tereshchenko, E.D., Grigoriev, V.F., Sergushin, P.A., Kopytenko, E.A., Biryulya, M.A., Skorokhodov, A.A., Esipko, O.A., and Damaskin, R.V., Electromagnetic sounding of the earth's crust in the region of superdeep boreholes of Yamal-Nenets Autonomous District using the fields of natural and controlled sources, *Izv., Phys. Solid Earth*, 2013, vol. 49, no. 6, pp. 844–858.

Zimin, E.F. and Kochanov, E.S., *Izmerenie parametrov elektricheskikh i magnitnykh polei v provodyashchikh sredakh* (Measurement of Parameters of Electrical and Magnetic Fields in the Conducting Earth), Moscow: Energoatomizdat, 1985.

Translated by E. Maslennikova